Hydrothermal Synthesis of Submicron- to Nano-Sized Ferroelectric Powders: Properties and Characterization

Sukon Phanichphant[1] and Robert Bertram Heimann[2*]

[1]Department of Chemistry, Chiang Mai University, Chiang Mai 50200, Thailand

[2]Department of Mineralogy, Technische Universitaet Bergakademie Freiberg, Freiberg, Germany

*Corresponding author. E-mail: heimann@mineral.tu-freiberg.de

ABSTRACT

Ferroelectric ceramics play an ever-increasing role as materials for electrical and electronic applications including multilayer capacitors (MLCs), dielectric resonators for frequency stabilization of microwave circuits, low-noise oscillators and low-insertion-loss bandpass filters for microwave communication components, dielectric waveguide resonators, piezoelectric transducers and sensors, piezomechanical actuators and motors, PTC thermistor, and a large variety of novel-emerging utilizations. The dielectric and electromechanic coupling properties of such ferroelectric ceramics are generally dependent on (i) dielectric permittivity, (ii) mechanical Q-factor and (iii) temperature coefficients of both resonance frequency and dielectric permittivity. These parameters in turn depend crucially on phase purity, impurity content, grain size and grain size distribution of the ceramic starting powder used to fabricate monolithic devices. Powder synthesis is customarily achieved by classical ceramic processing routes such as solid state reactions of constituent oxides, carbonates or nitrates. However, increasingly such methods are being employed that avoid repeated mixing, grinding and calcination steps through synthesizing the desired compositions from true or quasi-homogenous solutions by coprecipitation of hydroxides, sol-gel phase transition, or hydrothermal methods. Submicron- and nano-sized ferroelectric powders with favourable properties, synthesized by the latter method at the Department of Chemistry, Chiang Mai University and the Department of Mineralogy, Technische Universitaet Bergakademie Freiberg will be described in this contribution.

INTRODUCTION

Ferroelectrics are utilized as important components of a large variety of modern electric and electronic devices. As in all functional advanced ceramics, the performance of the endproduct will be determined to a large extent by the synthesis methods and hence properties of the ceramic precursor powders. In this contribution, the basic properties and physical underpinnings of ferroelectric materials will be discussed, as well as details on the hydrothermal synthesis of submicron- to nano-sized ferroelectric powders and their properties. Special emphasis will be devoted to research work performed jointly at the Department of Chemistry, Chiang Mai University, Thailand and the Department of Mineralogy, Technische Universitaet Bergakademie Freiberg, Germany.

ELECTRIC POLARIZATION IN DIELECTRIC MATERIALS

In contrast to metals with their typically high electrical and thermal conductivities, ceramics and most polymeric materials are so-called dielectrics. While in metals, the electrons are delocalized and randomly distributed ('electron cloud' model) and hence can freely movethrough the lattice in response to an outer electric field. In predominantly-covalent and ionic-bonded ceramics, the electrons are tightly bound to the atomic core. Hence in an ideal dielectric material, there is no long-range transport of charge carriers but only displacement of electrons, ions or dipoles relative to their equilibrium positions in the lattice. Consequently in ceramics, the electronic conductivity takes a distant second place to ionic conductivity. The degree of displacement corresponds to the restoring force excerted by the outer electric field that may be compared in a mechanical analogon to the restoring force of an extended spring. Since positive and negative charges will be displaced in opposite directions the crystal *acquires a dipole momentum* **p;** the macroscopic dipole momentum per unit volume is the *polarization*

$$\mathbf{P} = \varepsilon_0 \, \chi^e \, \mathbf{E}, \tag{1}$$

with the dielectric permittivity of the vacuum ε_0 (= $8.854 \cdot 10^{-12}$ As/(Vm)), the dielectric susceptibility χ^e, and the macroscopic electric field strength in the dielectric, **E.** The susceptibility is an anisotropic material constant and links the two vectors **P** and **E.** Hence it can be described by a (polar) symmetric tensor of 2nd rank ($\chi^e_{ij} = \chi^e_{ji}$). In the triclinic crystal system, the tensor of the dielectric susceptibility has six independent components. With increasing crystal symmetry, this number reduces and shows for tetragonal, rhombohedral or hexagonal crystals only two independent tensor components (χ^e_{11} and χ^e_{33}).

Polarization and susceptibility can be determined by measuring and comparing the capacities C of a capacitor with a dielectric (C) and an empty capacitor (C_0, in vacuum). The ratio C/C_0 is the *relative dielectric permittivity* $\varepsilon_r = \varepsilon/\varepsilon_0$, where ε is the permittivity of the dielectric and $\varepsilon_0 = 8.8542 \cdot 10^{-12}$ AsV^{-1}m^{-1} is the absolute dielectric constant of the vacuum. For the isotropic case the susceptibility χ^e and the relative dielectric permittivity ε_r are related by

$$\chi^e = \varepsilon_r - 1 = \varepsilon/\varepsilon_0 - 1. \tag{2}$$

Hence both ε_r and ε are 2nd rank tensors and link the vector of the electric field strength **E** and the dielectric displacement vector **D** by

$$\mathbf{D} = \varepsilon_0\varepsilon_r\mathbf{E} = \varepsilon\mathbf{E} \tag{3a}$$

and with eq. (1) and (2)

$$\mathbf{D} = \varepsilon_0\mathbf{E} + \mathbf{P}. \tag{3b}$$

From eq. (3a) it follows that the dielectric displacement **D** and hence the polarization **P** reduces to zero when the electric field disappears. However, there are crystals that display a so-called *spontaneous polarization* $\mathbf{P}_s$ already in the absence of an electric field, caused by the presence of singular (polar) directions in their crystal structures. This happens in the ten symmetry groups 1, m, 2, mm2, 3, 3m, 4, 4mm, 6 and 6mm (Table 1). It is important for our

further considerations to note that spontaneous polarization can also occur in polycrystalline ceramics with a polar symmetry group if an oriented arrangement exists of crystallites aligned by preferred texture.

The magnitude of the spontaneous polarization is temperature dependent

$$d\mathbf{P_s} = \mathbf{p}^*dT, \tag{4}$$

where $\mathbf{p}^*$ is the 'true' pyroelectric coefficient. The change of spontaneous polarization causes a charge displacement in response to changing temperature, *i.e.* opposite ends of a polar axis will be differently charged. This phenomenon is called the *'pyroelectric effect'*.

Table 1. Crystallographic classification with respect to crystal centrosymmetry and polarity (Uchino 1994).

Polarity	Centro-symmetry	Number of point groups	Crystal class												
			Cubic		Hexagonal		Tetragonal		Rhombo-hedral		Ortho-rhombic	Mono-clinic	Tri-clinic		
Non-polar (22)	O (11)	11	$m3m$ O_h	$m3$ T_h	$6/mmm$ D_{6h}	$6/m$ C_{6h}	$4/mmm$ D_{4h}	$4/m$ C_{4h}	$\bar{3}m$ D_{3d}	$\bar{3}$ C_{3i}	mmm D_{2h}	$2/m$ C_{2h}	T C_i		
	X (21)	11	432 O $\bar{4}3m$ T_d	23 T	622 D_6 $\bar{6}m2$ D_{3h}	$\bar{6}$ C_{3h}	422 D_4 $\bar{4}2m$ D_{2d}	$\bar{4}$ S_4	32 D_3		222 D2				
Polar (pyro) (10)		10			$6mm$ C_{6v}	6 C_6	$4mm$ C_{4v}	4 C_4	$3m$ C_{3v}	3 C_3	$2mm$ C_{2v}	2 C_2 m C_6	1 C_1		

*a* Piezoelectric crystals are those in the area enclosed by the thick line.

Some pyroelectrics have an additional property in that the direction of the spontaneous polarization can be changed by applying either an outside electric field or a mechanical stress. The former materials are called *ferroelectrics,* the latter *ferroelastics.*

FERROELECTRIC MATERIALS

Many important ferroelectric ceramics are based on the cubic perovskite structure with the general formula ABX_3 (Figure1) with X = O (oxygen). This structure consists of large A-type cations with low valency (K^+, Na^+, Ca^{2+}, Sr^{2+}, Ba^{2+}, Pb^{2+}, La^{3+}, Bi^{3+} and others) situated at the corners of the cubic unit cell, and small highly-charged B-type cations (Nb^{5+}, Ta^{5+}, Ti^{4+}, Zr^{4+}, Sn^{4+}, Ga^{3+} and others) in the center of the cubic unit cell surrounded octahedrally by six X ions that occupy the centers of the faces of the cubic unit cell. In titanate perovskites, the $[TiO_6]$ octahedra form chains parallel to the crystallographic z-direction (Figure.2). A- and B-sites can be occupied by cations of different valencies, thus leading to complex perovskites. For example, replacement of the B-site cation Ti^{4+} by $1/3Mg^{2+} + 2/3Nb^{5+}$ and the A-site cation by Pb^{2+} leads to the important ferroelectric relaxor ceramic PMN (lead magnesium niobate). On the other hand, the A positions can be shared
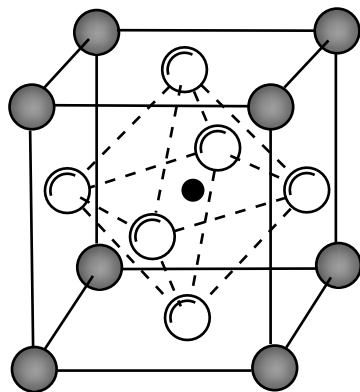
Figure 1. Ionic positions in ideal perovskite
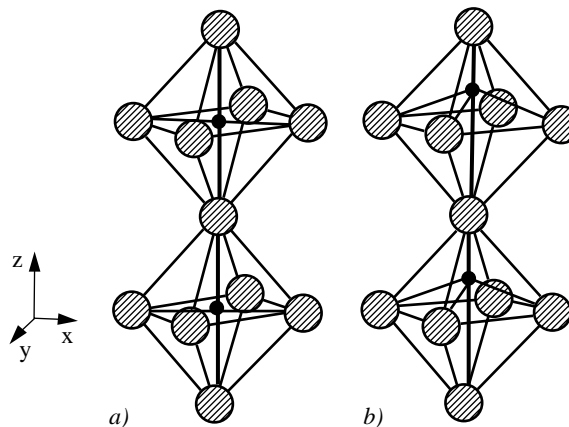
Figure 2. (a) [TiO_6] octahedra chain with a symmetry center above the Curie temperature T_C. (b) Ti-O-chain with spontaneous polarization in z-direction below T_C. The large circles denote oxygen ions, the small dots denote the B-type Ti^{4+} ion.

by dissimilar ions such as Na^+ and Bi^{3+}, yielding the complex ferroelectric relaxor ceramic BNT (bismuth sodium titanate) (see below).

The stability of the perovskite structure depends on Goldschmidt's tolerance factor $t = (r_A+r_O)/\sqrt{2}(r_B+r_O)$ with $0.7<t<1.2$. For tolerance factors outside this range, non-perovskite structure are stable, for example pyrochlore-type structures $A_2B_2X_6Z$, Aurivillius phases or tetragonal tungsten bronze (TTB)-type structures.

As evident from Figure 2b, displacement of the B-cation from the center of the oxygen octahedron in z-direction at a temperature below the Curie temperature introduces an asymmetric charge distribution within the coordination polyhedron and thus induces spontaneous polarization whose direction can be reversed by an outside electric field. In $BaTiO_3$ the displacement of the Ti^{4+} ion from the center of the coordination polyhedron in z-direction <001> causes a distortion of the originally-cubic symmetry m3m (space group Pm3m, No. 221) to a tetragonal symmetry 4mm (space group P4mm, No. 99) below 130°C. However, still other phase transitions have been observed in $BaTiO_3$. Around 0°C, distortion along the face diagonal <110> changes the symmetry group to orthorhombic (pseudo-monoclinic) mm2 (space group C2mm, No. 38), and at -90°C distortion along the space diagonal <111> changes the overall symmetry group to rhombohedral 3m (space group R3m, No. 160). Since the space groups mentioned are subgroups of Pm3m (the 'aristotype' according to Megaw, 1973), a so-called perovskite 'family tree' emerges (Bärnighaus, 1979). The electric nature of the cubic high-temperature phase with m3m symmetry above the Curie temperature $T_c = 130$°C is paraelectric. Figure 3 shows the temperature-dependent symmetry relations of barium titanate.
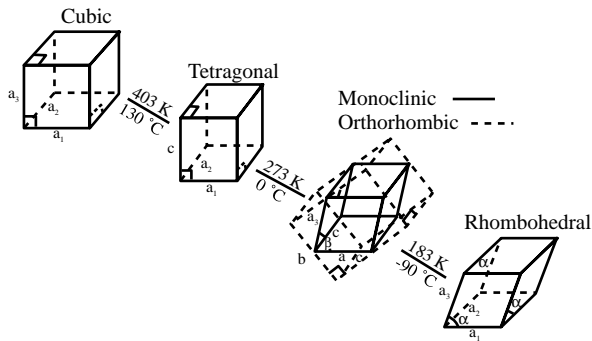
Figure 3. Unit cell distortions of single crystals of barium titanate (Kay and Vousdan, 1949)
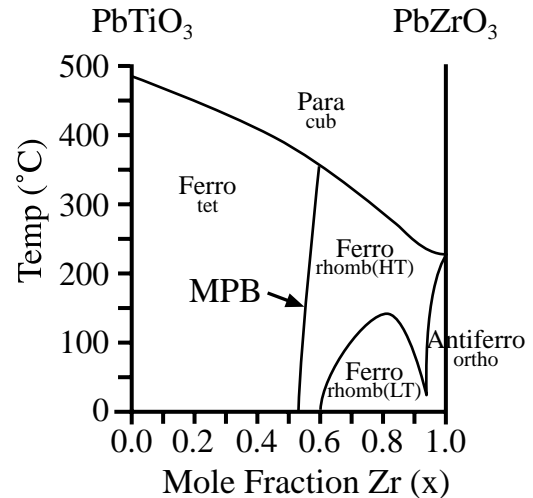
Figure 4. Phase diagram of the solid solution series $Pb(Ti_{1-x}Zr_x)O_3$. The ferroelectric tetragonal and rhombohedral phase fields are separated by the morphotropic phase boundary (MPB) (Heaney, 2000)

These structural relationships can be explained more clearly, using the ferroelectric (and piezoelectric) solid solution system of $Pb(Zr_xTi_{1-x})O_3$ (lead zirconate titanate, PZT). The two endmembers are $PbTiO_3$ that undergoes at 490°C a simple phase transition from a paraelectric cubic to a ferroelectric tetragonal phase, and $PbZrO_3$ that behaves in a more complex fashion, having a transition from cubic to an antiferroelectric orthorhombic phase. Replacement of Zr by Ti produces low-and high-temperature rhombohedral ferroelectric phases. Figure 4 shows the phase diagram of the solid solution system $Pb(Zr_xTi_{1-x})O_3$. Below the Curie temperature, the phase field of the ferroelectric states is separated by a near-vertical line, the *morphotropic phase boundary* (MPB).

The term 'morphotropism' was introduced by the German crystallographer von Groth already in 1870 and is defined as a structural change introduced by chemical substitution (von Groth, 1870). The morphotropic phase diagram, shown in Figure 4, belongs to type IV (Heaney, 2000) in which the space groups of the low temperature ferroelectric phases are subgroups of the paraelectric high-temperature phase. Much experimental work has confirmed that in the vicinity of the MPB properties such as electric susceptibility χ^e and thus dielectric permittivity ε reach anomalously high values (cp. Figure 8). This is usually explained by the large number of possible directions of polarization. Whereas in the region of the ferroelectric tetragonal structure, only 6 possible domain orientations exist conforming to the six <100> directions and in the region of the rhombohedral structure, 8 orientations commensurate with the eight <111> directions, near the MPB the ferroelectric domains adopt 14 orientations (6+8) for aligment during poling (Heywang, 1965).

The changes in polarization directions can be explained by invoking the concept of the polarizability α of ions. This quantity relates the dipol momentum **p** to the local field strength $\mathbf{E_L}$ that is associated with the deformation of the electron orbital shells of individual ions:

$$\mathbf{p} = \alpha \, \mathbf{E_L} \qquad\qquad (4)$$

According to Heywang (1951) the effective polarizability in crystals of perovskite structure is

$$\alpha = \alpha_A + \alpha_B + 3\alpha_O + \gamma\alpha_O, \qquad\qquad (5)$$

where the subscripts A, B and O refer to the combined electronic and displacement polarizabilities of the A-, B- and oxygen ions. The complex factor γ (Lorentz factor) considers the long-range Coulombic interactions in structures with non-cubic environment[1] and contains the scaling factors p = 0.69 and q = 2.39 to yield

$$\gamma = [q\,B^*+p(O^*-A^*)]^2/[(2/3)[1+pO^*]-O^*(q^2B^*+p^2A^*+p^2O^*/3), \qquad (6)$$

with $A^* = \alpha_A/\varepsilon_0 v$, $B^* = \alpha_B/\varepsilon_0 v$ and $O^* = \alpha_O/\varepsilon_0 v$ (v = volume of unit cell).

Owing to the high value of q, the polarizability of the B-ions combined with the likewise high polarizability of the oxygen ions contribute to a large extent to the effective (total) polarizability α. For the case of barium titanate, $A^* = 0.20$ leads to $\gamma = 1.38$ and $\varepsilon_r(0) = 26.6$. However, a very slightly larger $A^* = 0.21$ yields $\gamma = 1.73$ and hence $\varepsilon_r(0) \rightarrow \infty$, *i.e.*, a polarization catastrophe associated with a second-order ("λ"-type) ferroelectricñparaelectric phase transition at T_C (see Figure 5). This behaviour will be augmented by displacement of oxygen ions, causing a dynamic covalency. The latter occurs when B-sites will be replaced by small transition metal ions with unfilled d-orbitals that "rattle" around within the oxygen coordination polyhedron 'cage'. This will lead to asymmetric approaches of the B-ions to oxygen ions and hence an increase of the proportion of the covalent bonding force. The system reacts to that situation by partial charge transfer and consequently to an additional dipol momentum, causing the B-ions to move in a double-potential energy well structure[2] (Figure 6) leading to an OD (order-disorder) phase transition. An applied electric field enables a Ti^{4+} ion to overcome the shallow energy barrier 'hump' between the two equivalent energy states and consequently to move from one well into the other one, thus reversing the direction of polarity in this lattice region. By cooperative coupling, the energy increment required for a neighbouring unit cell to make the same transition will be reduced and eventually the entire domain, will switch to the new direction. Within a domain, the direction of spontaneous polarization is identical but differs from domain to domain.

Since the orientation of domains can be deduced from the (higher) symmetry of the paraelectric 'aristotype' phase, the domains are structurally related to each other by twin planes obeying appropriate twin laws, usually 180°-domains. In some ferroelectric materials, noticeably barium titanate, there exist also 90°-domains that originate from mechanical stress associated with the phase transition by domain movement and hence are induced by the ferroelastic effect (Nord, 1994).

Not only the high polarizability of the B-ions but also a higher polarizability of A-ions favour ferroelectric behaviour. So is the Curie temperature of $PbTiO_3$ considerably higher ($T_C = 490°C$) than that of $BaTiO_3$ ($T_C = 130°C$) since $\alpha_{A(Pb)} = 1.4\,\alpha_{A(Ba)}$. The anharmonicity of

---

[1] For structures with cubic environments, the interaction is given by the well-known Clausius-Mosotti equation.
[2] In terms of Thom's (Thom, 1975) catastrophe theor,y this double-energy well structure corresponds to a cusp catastrophe of codimension 2 (Riemann-Hugoniot catastrophe).

the perovskite lattice leads to a decrease of polarizability with increasing temperature ($\delta\varepsilon/\delta T < 0$) and in turn to a disappearing of ferroelectricity at the Curie temperature (Figure5). The material becomes paraelectric and then the relative dielectric permittivity ε_r obeys the Curie-Weiss law, $\varepsilon_r = C/(T-T_C)$.
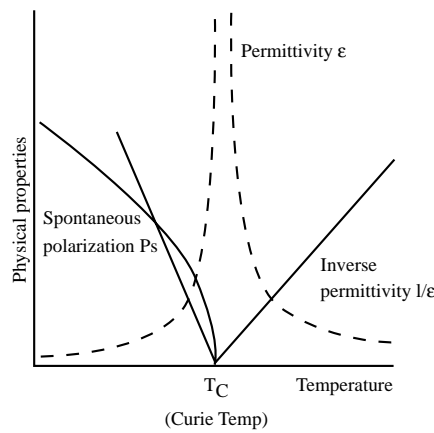

Figure 5. Temperature dependence of spontaneous polarization $\mathbf{P}_S$ and dielectric permittivity ε_r of a ferroelectric ceramic in the vicinity of the Curie temperature T_C.
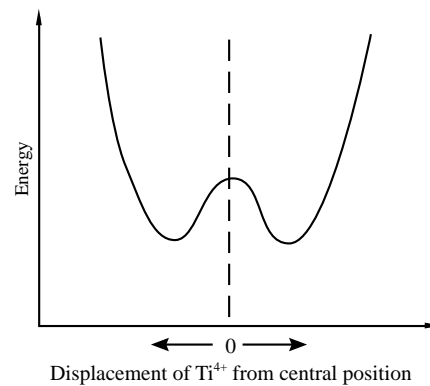
Figure 6. Double-energy well structure of Ti^{4+} along the z-axis (Moulson and Herbert, 1990)

The fact that an electric field can reverse the direction of spontaneous polarization by cooperative movement of domain walls requires an energy contribution that the dielectric material takes from the surrounding electric field. In an oscillating a.c.field, the phase shift between current and voltage in the absence of a dielectric is exactly 90˚. Introducing a ferroelectric material results in a slightly smaller phase shift 90˚-δ, where δ is the angle of dielectric loss, and $1/\tan\delta \equiv Q$, the 'mechanical' quality factor. The Q factor plays an important role in electrical resonance since the sharpness of tuning increases with increasing Q factor by decreasing the damping function. Application of a strong static electric field to a polycrystalline ferroelectric ceramics at elevated temperature can permanently fix the direction of the domain orientation, *i.e.* the direction of polarization. This process is called 'poling'. Plotting the polarization against the electric field strength yields the typical hysteresis loop of a ferroelectric material (Figure7). After switching off the field, a part of the
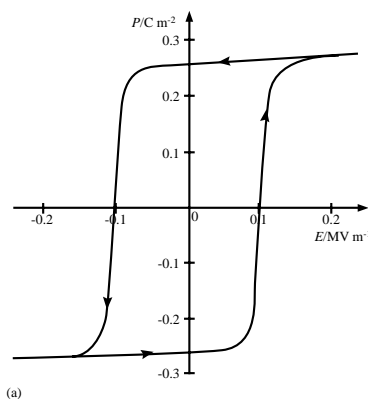
Figure 7. Hysteresis loop for a single-domain single crystal of barium titanate (Moulson and Herbert, 1990).
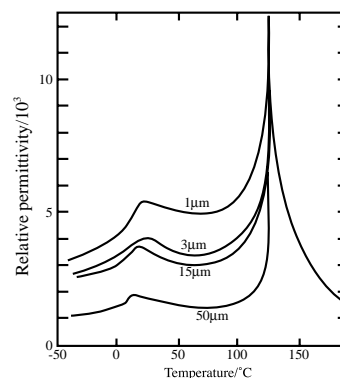
Figure 8. Dependence of relative permittivity of grain size of BaTiO3. (Kinoshita and Yamaji, 1976)

preferential domain orientation will be retained (remanent polarization). To remove this remanent polarization, a reverse electric field with a coercitive strength E_C must be applied in order to reproduce the original (statistical) domain orientation ($P = 0$).

The near vertical portions of the loop in Figure 7 correspond to the reversal of the spontaneous polarization when opposite 180°-domains nucleate and grow. The near horizontal portions represent saturated single domain states. The remanent polarization shown is about 0.27 C/m^2, the coercitive field strength (-)0.1 MV/m.

The ease with which poling occurs points to not-very-stable structural states that make possible a displacive phase transitions from low temperature ferro- to high temperature paraelectric, or antiferroelectric to ferroelectric states. The phase transition can be described as a swinging motion of the B-ion through the plane of the four oxygen atoms in the center of the oxygen coordination polyhedron (see Figure 1). The frequency of these 'soft' mode phonon vibrations decreases by approaching the transition temperature and 'freeze' at the Curie temperature in a polar, *i.e.* ferroelectric configuration[3]. This behaviour causes high polarizabilities of the TiO_6-octahedra that result in anomalously high values of the dielectric permittivities (Figure 5), as well as the electro-optical, non-linear optical, piezoelectric and electromechanical coupling coefficients (Cross, 1993). This is at the very heart of technical applications of ferroelectric materials as ultrasonic oscillators, acoustic and optical frequency multipliers, dielectric amplifiers, acoustic and optical frequency modulators, switches, sensors, actuators and many more. For a contemporary account on these applications see Cross (1993) and Uchino (1994).

Experimental evidence exists that the grain size of a polycrystalline ferroelectric ceramic strongly influences the crucial dielectric properties such as permittivity, electromechanical coupling coefficient, *i.e.* the efficiency of conversion of mechanical into electrical energy and *vice versa,* and in particular the electro-optical behaviour. Figure 8 shows an example of the dependency of the relative dielectric permittivity ε_r of $BaTiO_3$ on the grain size between 1 and 50 µm. The figure shows that ε_r strongly increases with decreasing grain size at the Curie temperature and also increases in the vicinity of the tetragonal-orthorhombic phase transition around 0°C, thus raising the permittivity level below T_C. To attain small grain sizes during conventional solid state powder sintering, doping plays an important role as substitution with higher valency ions, *e.g.* La^{3+} for Ba^{2+}, and Nb^{5+} or Al^{3+} for Ti^{4+} inhibits grain growth. However, producing nano-sized ferroelectric powders by a hydrothermal route will go a long way towards very fine-grained sintered monolithic bodies. The principles of hydrothermal powder processing will be described in the following chapter.

---

[3] In a more complex treatment, this soft optical phonon mode is a RUM (= rigid unit mode) where the BO_6 octahedra of the perovskite structure are taken as rigid units that rotate by the angle Φ around their vertices to attain phase transition (Dove et al., 2000). The softening of the transverse optical (TO) phonon mode causes the frequency of the associated transverse acoustic (TA) branch to be depressed with increasing wave vector k to zero frequency close to $k = 0$. As a result, an incommensurate displacive phase transition occurs (Tautz et al., 1991). The angle of rotation Φ of the RUM octahedra is the order parameter Q in the Landau-Ginzburg theory of phase transition (Landau and Lifshitz, 1980) that converges towards zero when the Curie temperature is reached (Carpenter, 1992).

HYDROTHERMAL POWDER PROCESSING

Hydrothermal processing involves (chemical) reactions occuring at elevated temperature and pressure conditions (T >100˚C, p > 100 kPa) in aqueous solutions within a closed system (Yoshimura and Suda, 1994). Hence this technique successfully closes the gap between materials processing at low to ambient pressure and high to ultrahigh pressure in a temperature range between 100˚C and about 1600˚C (Figure 9).

In contrast to other more conventional techniques, hydrothermal synthesis offers several advantages including (i) synthesis in a closed system of compounds with elements in varying valence states such as transition metal compounds, (ii) synthesis and crystal growth of phases stable at low temperature, (iii) synthesis and processing of metastable compounds, (iv) high growth rates of single crystals owing to the high mobility of ions and ionic complexes under hydrothermal conditions, (v) synthesis of powders with high purity in the presence of inert autoclave liners (platinum, gold, PTFE), (vi) environmental friendliness since carried out in a closed system, and (vii) synthesis of ultrafine, crystalline, frequently spherical, uniform powders that may not, in the case of ferroelectrics, require subsequent calcining and conditioning steps before sintering.
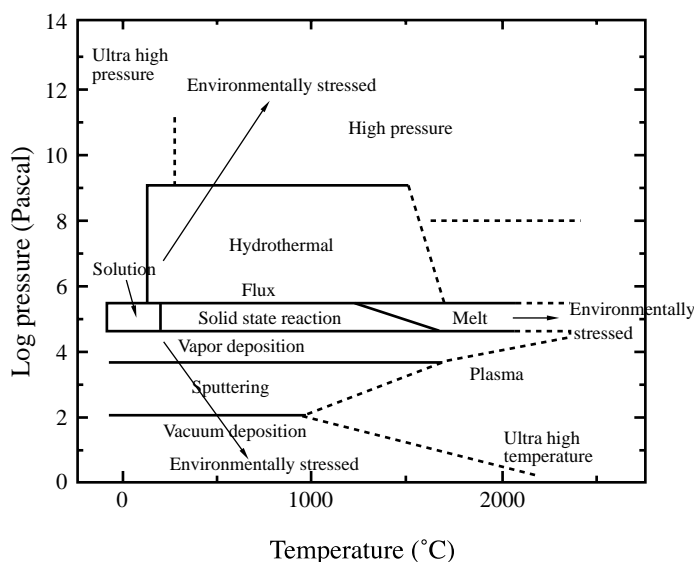
Figure 9. Temperature-pressure range for materials processing (Byrappa and Yoshimura, 2001).

Table 2 shows a comparison of different advanced powder synthesis routes (Dawson 1988; Cousin and Ross, 1990). It should be emphasized that frequently co-precipitation/calcination or sol-gel synthesis are being used to produce precursor powders with a high control in stoichiometry that subsequently are being hydrothermally recrystallized to yield submicron- to nano-sized highly crystalline particles for utilization in advanced electronic devices.

Table 2. Comparison of different advanced powder synthesis routes (after Dawson 1988, Cousin and Ross, 1990).

Method*	Composition control#	Morphology control	Powder reactivity	Particle size (nm)	Purity (%)	Agglome-ration	Calcina-tion	Milling	Cost
A	-	-	-	>1000	<99.5	0	yes	yes	-/0
B	+	0	+	>10	>99.5	+	yes	yes	0
C	++	0	+	>10	>99.9	-	no	no	0/+
D	++	++	+	>100	>99.9	-	yes	yes	0
E	++	++	+	>10	>99.9	-	no	no	+
F	++	0	+	>10	>99.9	0	yes	yes	+
G	*++*	*+*	*+*	*>10*	*>99.5*	*-*	*no*	*no*	*0*

* A: solid state reaction, B: Co-precipitation, C: spray- or freeze-drying, D: emulsion synthesis, E: spray pyrolysis, F: Sol-gel. G: hydrothermal.
# - : poor, low; 0 : moderate, + : good, high, ++ : excellent

From Table 2 it follows that hydrothermal synthesis of ceramic powders provides two major advantages: (i) the elimination or at least minimization of any high temperature calcination or conditioning steps and (ii) the utilization of relatively-inexpensive precursor materials. While generally not limited to oxide compounds, the technique is particularly suitable for preparing not only advanced functional ceramic powders such as PZT or BNT as well as a wide range of magnetic ferrite oxides with magnetoplumbite or spinel structures but also advanced structural oxide ceramics such as alumina and zirconia. Consequently, hydrothemal synthesis will find its commercial niche precisely in the area of producing advanced electronic ceramics if process-related and economic obstacles can be successfully overcome in the future.

To weigh the advantages and disadvantages of hydrothermal powder processing, the following aspects may be considered (Ponton, 1993).

(1) The process utilizes comparatively inexpensive precursor chemicals such as oxides, hydroxides, chlorides, acetates and nitrates rather than the expensive alkoxides required for sol-gel processing.

(2) Reactants that are normally volatile at the required reaction temperature tend to condense during the hydrothermal process and thus maintain the reaction stoichiometry. Consequently, highly pure, multicomponent anhydrous ferroelectric powders can be obtained.

(3) Hydrothermal synthesis is a low-temperature process with many effects achievable even below 300°C. The relatively low temperature can break down stable precursors under pressure, thus avoiding the extensive agglomeration that solid state reactions usually cause at high sintering temperature.

(4) The process is amenable to produce solid solution particles with controlled size distribution, shape, and complex chemical composition. Multi-doped perovskite ABO_3 ceramic powders, for example, can be grown down to submicrometer or even nanometer size by close control of the nucleation and growth steps.

(5) Powders grown by the hydrothermal process rarely require presintering or calcination steps. This is particularly important for synthesizing high quality PZT powders since lead oxide is quite volatile at conventional calcination or sintering temperatures.

(6) Synthesis is accomplished in a closed system from which different chemicals can be recovered and recycled, thus making it an environmentally-benign technology.

(7) The process can be easily scaled up to industrial demand since hydrothermal synthesis in principle lends the opportunity for cost effective and reproducible production of high quality ceramic powders on a large industrial scale.

These decisive advantages have to be judged against the following disadvantages of the hydrothermal processing technology:

(1) Comparatively high initial cost of the equipment such as autoclaves, liners, valves, pressure tubing, control equipment and other ancilliary tools.

(2) Requirement of a stringent safety regime caused by the high pressure applied, *i.e.* appropriate shielding and utilization of burster disks *etc.*

(3) Potential high temperature corrosion problems arising from the presence of alkaline or acidic mineralizers that require inert noble metal or polymeric autoclave liners.

(4) Closed autoclaves do not normally allow to visually observe the progress of the reaction. Application of transparent windows of corrosion-resistant materials such as alumina, magnesia or spinel is possible but adds to the cost since they have to be frequently replaced.

Beside these considerations, the theoretical aspects of hydrothermal materials processing are still somewhat obscure in spite of decades of successful application to a large variety of compounds including ferroelectrics. The fundamentals of solubility, nucleation, phase equilibria, thermodynamics, kinetics, modeling and intelligent engineering are still in the process of being developed so that a consistent picture is sadly missing to date. The dependence of the solubilities of precursor compounds in an aqueous environment at higher temperature and pressure on the concentration of mineralizers, and the decisive role that temperature, pressure, choice of precursor compounds and time play on the crystallization kinetics of perovskite powders has been studied in detail by Riman and co-workers (for example Lencka and Riman, 1995a; Lencka et al., 1995; Riman et al., 1996; Riman et al., 1997). In fact, these authors have successfully developed a novel approach to transform hydrothermal synthesis from an empirical laboratory technique to a thermodynamically based technology, using principles of intelligent engineering (Byrappa and Yoshimura, 2001). With this they attempted to decouple the interplay between thermodynamics and kinetics (Lencka and Riman, 1995b). For example, Figure 10 shows calculations performed in the temperature-pressure-composition (T-P-X) space, indicating the stability fields and speciation of lead titanate as well as the yield under hydrothermal conditions as a function of the pH of the solution.

Two basic kinetic models have been proposed to describe the formation of perovskite-type materials under hydrothermal synthesis conditions. The *in situ reaction*

mechanism proposes a reaction of solid TiO_2 or ZrO_2 grains with dissolved A^{2+} ($A = Ba^{2+}$, Pb^{2+},...) species to form a continuous layer of perovskite of various stoichiometries until the supply of the solid has been exhausted. The reaction layer serves as a diffusional barrier to slow down or even halt the hydrothermal reaction. The *dissolution-reprecipitation mechanism* (Figure 1 1) is more complex, requiring breaking of Ti-O or Zr-O bonds by hydrolytic attack to form hydroxide complexes of type $(Ti,Zr)(OH)_x{}^{4-x}$ that are able to react in solution with A^{2+} ions or AOH^+ complexes via homogenous or heterogeneous nucleation to form $A(Ti,Zr)O_3$. When heterogeneous reactions occur, the consequences are similar to those encountered with the *in situ* mechanism: formation of a diffusional barrier that interferes
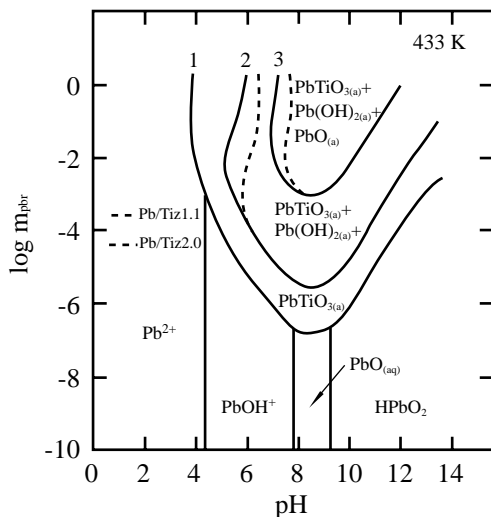
Figure 10. Stability, speciation and yield diagram of lead titanate under hydrothermal conditions (Eckert et al., 1996).
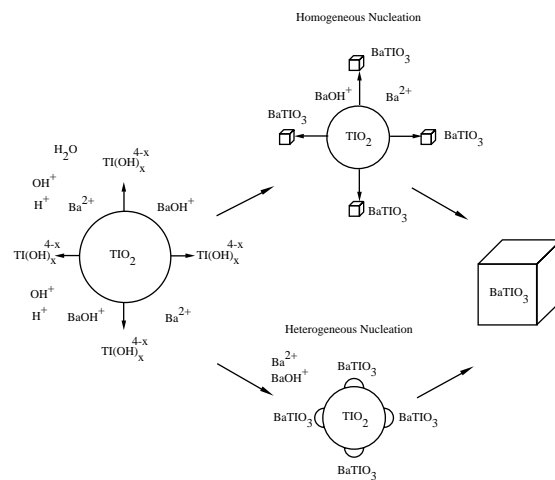
Figure 11. Dissolution-reprecipitation reaction mechanism of hydrothermal synthesis of barium titanate (Eckert el al., 1996)

with the kinetics of the hydrothermal reaction. To ensure homogeneous nucleation, a hydrous TiO_2 or ZrO_2 reactant must be chosen that bypasses most of the limiting hydroxylation steps. This requires the use of titanium or zirconium alkoxides or hydroxides.

As examples, the following chapter will outline details of hydrothermal syntheses of nano-sized powders of important ferroelectric ceramics such as PZT (lead zirconate titanate) and BNT (bismuth sodium titanate) carried out jointly at the Department of Chemistry of Chiang Mai University, Thailand and the Department of Mineralogy, Technische Universität Bergakademie Freiberg, Germany.

HYDROTHERMAL SYNTHESES OF NANO-SIZED PEROVSKITE POWDERS

To demonstrate the suitability of hydrothermal processing to obtain ferroelectric powders with technically-useful properties in this chapter, two typical materials will be discussed: the 'normal' ferroelectric ceramic lead zirconate titanate (PZT) and the relaxor ferroelectric ceramic bismuth sodium titanate (BNT).

Lead zirconate titanate (PZT)

The most commonly-used precursors for hydrothermal synthesis of PZT powders are nitrates, chlorides, oxychlorides, acetates, hydroxides, as well as Zr and Ti alkoxides. The compositional ratio of Ti/Zr is generally around 0.48/0.52 to assure that the desired composition $PbZr_{0.52}Ti_{0.48}O_3$ is close to the morphotropic phase boundary (MPB) zone in the phase diagram of the binary system $PbTiO_3$-$PbZrO_3$ (see Figure 4). For a definition of the MPB see above. Owing to the amphoteric nature of PbO, some of it will remain in solution after the hydrothermal reaction. Reports indicate (Ichihara et al., 1999) that addition of about 22% excess of a lead compound was required to obtain stoichiometric PZT powders. Excess lead has also been used to compensate for the evaporation losses during subsequent sintering required to obtain better electric properties (Lin et al., 1993) and products with a low degree of agglomeration (Lemoine et al., 1995).

Generally, a catalyst or 'mineralizer' is required to increase the solubility of the precursor compounds. The use of strong alkalis such as KOH or NaOH, or halides such as KF, LiF. NaF or KBr has been reported (Beal, 1987). However, it was noted that lithium and fluorine, in combination or separately, were selectively retained as impurities in PZT. In addition, they also tend to increase the degree of retention of other alkalis or halides. The concentration of catalysts/mineralizers strongly influences the PZT formation. During the initial stage of PZT formation (see Figure 10) at lower KOH concentration (*e.g.* < 2 mol/l), only $PbTiO_3$ and $PbZrO_3$ were formed. However, at higher KOH concentrations (*e.g.* > 4 mol/l, PZT was produced and the rate of production increased with increasing concentrations (Lee et al., 1987). Since the individual Pb, Ti and Zr ion species show different solubilities with increasing alkalinity of the hydrothermal solution, their interactions become quite complex. It is for this reason that the mechanisms of formation of PZT from hydroxides have not been elucidated in all their details at present. Moreover, the types of alkali used also play an important, yet not completely understood, role during morphological development of PZT particles. For example, using KOH as a catalyst, the PZT powder particles tend to be cube-shaped while using NaOH results in tabular particles with increased grain size (Lemoine et al., 1995). Other studies indicate that PZT and PLZT powders could not be formed without KOH catalyst even at temperatures as high as 400˚C (Nualpralaksana et al., 2001). This, however, is in contrast to results reported earlier (Kutty and Balachandran, 1984). According to Su (1997), the critical concentration of KOH to form PZT was 0.4 mol/l. Below this concentration only $PbTiO_3$ was formed as the dominant phase. However, cubic PZT was formed when NaOH was used at concentrations, as low as 0.3 mol/l. This suggests that the catalytic properties of the alkali mineralizer are not only determined by the pH values achieved in solution but also by the size of the alkali cation. The cation with the smaller radius (Na) will encounter less steric hindrance and hence will diffuse more readily, thus assisting in PZT formation.

Another important factor influencing the mechanism of hydrothermal formation of PZT powder is temperature. This factor, however, is not an independent one but interacts in a nonlinear fashion with the mineralizer type and its concentration. Experiments have shown that the rate of nucleation of PZT decreases with increasing temperature but that sufficient crystal growth rates can still be achieved at temperatures as low as 150˚C (Dawson, 1988). Below 130˚C in the presence of 3 mol/l KOH, the product was tetragonal PbO together with

an undisclosed amorphous phase whereas a mixture of crystalline Ti-rich tetragonal and Zr-rich rhombohedral PZT appeared above 150°C (Cheng et al., 1993). This finding is in part supported by a study showing the formation of fine spherical powders of 200-300 nm size with a 1:1 mass ratio of tetragonal $PbZr_{0.52}Ti_{0.48}O_3$ and rhombohedral $PbZr_{0.58}Ti_{0.42}O_3$ phases, synthesized in the presence of 4 mol/l KOH at temperatures around 140°C and pressures of 500-600 kPa for 3-5 hours (Nualpralaksana et al., 2001). As shown in Figure 12, left panel the as-synthesized PZT sample shows broad interplanar spacings pointing to a very small grain size of the (spherical) product. In addition to the target composition, there occurs a pyrochlor-type $Pb(II,IV)_2[Ti_xZr_{1-x}]_2O_7$ phase, denoted by a dot. After calcination at 800°C (Figure 12, right panel) the pyrochlor-like phase has disappeared, and the final PZT product consisted of a mixture of 51.4 ± 3.3 mass% of the tetragonal $PbZr_{0.52}Ti_{0.48}O_3$ and 48.6 ± 3.3 mass% of the rhombohedral $PbZr_{0.58}Ti_{0.42}O_3$ phases.
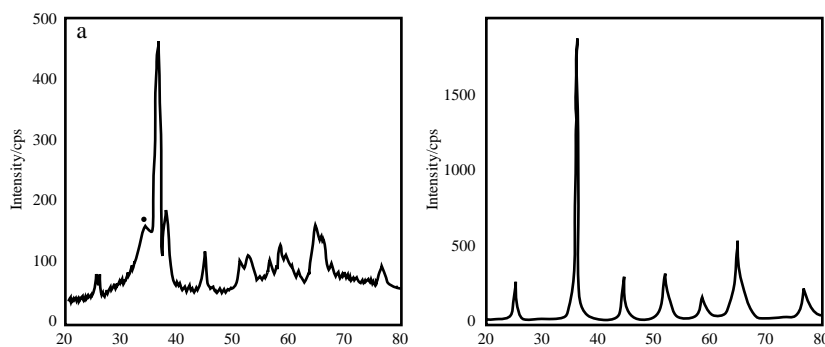
Figure 12. XRD pattern of PZT hydrothermally synthesized at 125°C, 600 kPa, pH = 13 for 5 hours (left) and calcined for 2 hours at 800°C in air (left) (Nualpralaksana et al., 2001).

Above a synthesis temperature of 250°C, submicron- or even nano-sized PZT powders can still be formed even at low catalyst concentrations. For example, PZT formation was confirmed in the presence of 1 mol/l KOH (Lemoine et al., 1995), at a rather low pH of 9.5-9.7 (Adschiri et al., 1992) as well as at 0.1 to 0.66 mol/l alkali concentrations (Beal, 1987).

Bismuth sodium titanate (BNT)
This ferroelectric material of complex perovskite-type structure was originally discovered by Smolenskii et al. already in 1961. It is of potential interest as a material to replace the widely-used but environmentally-problematic lead-based perovskites since (i) it does not pollute the environment with toxic lead and (ii) its synthesis does not require a controlled atmosphere. BNT has a Curie temperature T_c of 320°C, and its dielectric displacement-electric field strength (D-E) hysteresis loop shows a remanent polarization of $P_r = 0.38$ C/m² and a very high coercive field strength of $E_c = 7.3$ MV/m (cp. Figure 7) at ambient temperature where a rhombohedral ferroelectric phase is stable (Hosono et al., 2001). This phase transforms at 200°C to an antiferroelectric phase (Aparna et al., 2002). Since the existence of a rhombohedral phase suggests the possibility to obtain a MPB in combination with another ferroelectric compound with tetragonal structure, it was not surprising that such a complex composite ferroelectrics was eventually found by Takenaka and Sakata (1989) by doping BNT with 6 at% of barium to yield $(Na_{1/2}Bi_{1/2})_{0.94}Ba_{0.06}TiO_3$ with a rather small dielectric constant $\varepsilon_{33} = 580$ but a high electromechanical coupling coefficient $k_{33} = 55\%$ and

a high mechanical strength of $\sigma = 200$ MPa. It was also reported in the literature that within the solid solution series $(NaBi)_{1/2}TiO_3 – (KBi)_{1/2}TiO_3$ a morphotropic phase boundary exists in the range of 16-20 mol% tetragonal $(KBi)_{1/2}TiO_3$ where the piezoelectric constant d_{33}, the elastic compliance s_{11} and the electromechanical coupling coefficient k_{31} peak at 47 pC/N, 8.8 pm^2/N and 20%, respectively (Sasaki et al., 1999).

In contrast to PZT described in the preceding paragraph, BNT is a ferroelectric relaxor ceramic. Ordering of Bi and Na causes structural chemical inhomogeneities that result in the formation of nanometer-scaled domains of comparable orientation (Känzig, 1951). Owing to thermal motions close to the diffuse order-disorder (OD) phase transformation, polarization fluctuations exist among these domains. Since tighly coupled dipoles within Bi-rich domains act like superparaelectrics (Schmidt et al., 1994), their reorientation under the influence of temperature variations, caused by the surrounding electric field, produces large dielectric permittivities and large electrostrictive effects. This is a hallmark of ferroelectric relaxor ceramics (Newnham and Ruschau, 1991). Hence complex ferroelectric relaxor ceramics such as BNT (bismuth sodium titanate), PMN (lead magnesium niobate) or PZN (lead zinc niobate) are characterized by a very diffuse range of the ferroelectric-paraelectric OD phase transition (see Figure 14, left panel).

All previously-reported BNT ceramics were prepared by conventional processing routes, including sintering of mixed powders (Herabut and Safari, 1997; Nagata and Takenaka, 1997; Wada et al., 2001) and, for single crystal growth, flux and Bridgman methods (Hosono et al., 2001). However, hydrothermal synthesis of BNT was used by Pookmanee et al., (2001, 2003) to obtain near single-phase powders by processing highly-alkaline mixtures of bismuth nitrate, sodium nitrate and titanyl nitrate in PTFE-lined autoclaves of 500 ml volume and a degree of filling of 25% at 200°C for 24 hours. This treatment resulted in the formation of spherical particles of rhombohedral structure with space group R3m and diameters ranging between 200 and 800 nm (Pookmanee et al., 2001). During post-synthesis sintering of (nearly) phase-pure BNT, it was observed that already at temperatures as low as 1000°C, substantial decomposition occured. Actually, sintering for 3 hours completely destroyed the ferroelectric BNT phase and the resulting product was composed of a mixture of the paraelectric pyrochlor-type phases $Bi_2Ti_2O_7$ and $BiNaTi_6O_{14}$ (= $[(BiNa)_{0.5}Ti]Ti_2O_7$), formed by partial evaporation of sodium and bismuth oxides according to

$$4 (BiNa)Ti_2O_6 \rightarrow Bi_2Ti_2O_7 + BiNaTi_6O_{14} + 3/2\ Na_2O\uparrow + {}^1\!/_2\ Bi_2O_3\uparrow$$

To prevent this undesirable decomposition, it was sufficient to add as little as 1at% La as a dopant to stabilize the structure of BNT, during sintering. Indeed, the XRD pattern of La-doped BNT sintered at 1000°C for 3 hours, showed a mixture of rhombohedral ferroelectric and tetragonal antiferroelectric BNT, phases (Figure 13), in contrast to the results reported by Herabut and Safari (1997) who found that BNT doped with 2 at% La still retained its rhombohedral R3m structure but with only a slight change in axial length and lattice angle parameters. The tetragonal BNT phase found by Pookmanee et al., (2003) appears at the low angle flank of the interplanar spacings of the rhombohedral phase as revealed by pronounced line splitting.
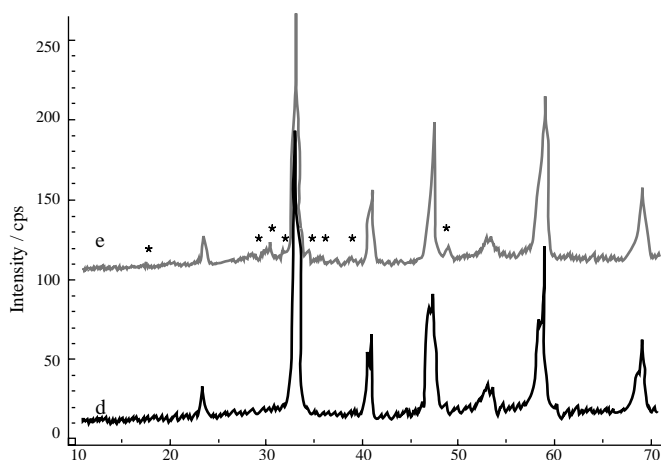
Figure 13. XRD pattern of hydrothermally-synthesized BNT powder doped with 1 at% La (d) and 2 at% La (e), sintered at 1000˚C for 3 hours. The sample doped with 2 at% La shows small amounts of $BiNaTi_6O_{14}$ (asterisks) as thermal decomposition product. CuK α, 40 kV, 40 mA, automatic divergence slit (Pookmanee et al., 2003).
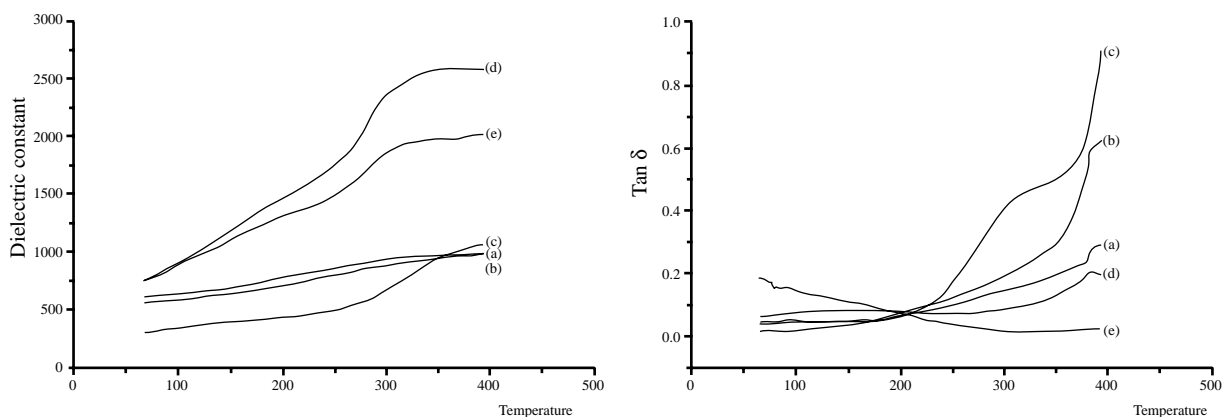
Figure 14. Dielectric permittivities (left panel) and dielectric loss tangents (right panel) of sintered undoped BNT (a-c) and La-doped BNT (d,e) measured at 1 kHz (Pookmanee et al., 2003).

Figure 14 (left panel) shows the temperature variation of the dielectric permittivity of hydrothermally-synthesized undoped BNT samples (a: sintered for 1 h; b: sintered for 2 h; c: sintered for 3 h) as well as BNT doped with 1 at% La (d: sintered for 3 h) and 2 at% La (e: sintered for 3 h). All samples were sintered at 1000˚C and measured at a frequency of 1 kHz. Figure 14b shows the dielectric loss tangent of the same samples.

While the dielectric permittivities of the undoped BNT samples vary approximately linearly with temperature and hence do not follow the Curie-Weiss law, the sample sintered for 3 hours (c) shows a surprising deviation from linearity, starting around 250˚C. An explanation for this can be found, considering a higher degree of sintering with associated reduction of grain boundaries and hence a reduced degree of relaxation of space charge polarization and phonon scattering. On the other, hand due to retention of the ferroelectric rhombohedral phase in La-doped samples (d,e), the dielectric permittivities of these samples increase strongly with temperature to about 350˚C, in concurrence with a diffuse OD phase

transformation typical for a ferroelectric relaxor material that accounts for the broad maximum in strong contrast to the behaviour of normal ferroelectric ceramics such as PZT (cp. Figure 8). In addition, relaxor ceramics such as BNT show a dielectric relaxation, *i.e.*, a frequency dependence of the dielectric permittivity as well as the dielectric loss tangent (Pookmanee et al. 2003), presumably related to the locally-disordered domain structure that creates shallow multipotential wells (Skinavi et al., 1961).

Figure 14 (right panel) shows the temperature dependence of the dielectric loss tangent of the samples. In the undoped samples a-c, the loss tangent increases strongly with temperature and sintering time in concurrence with the progressive destruction of the ferroelectric rhombohedral phase. While this also holds for the BNT samples doped with 1 at% La (d), the sample doped with 2 at% La (e) shows a monotonous decrease of the loss tangent with temperature and reaches a value of close to $\tan \delta = 0$ near the Curie temperature.

REFERENCES

Adschiri, T., K. Kanazawa and K. Arai. 1992. Rapid and continuous hydrothermal crystallization of metal oxide particles in supercritical water. J. Am. Ceram. Soc. 75: 1019-1022.

Aparna, M., T. Bhimasankaram, G.S. Kumar and G. Prasad. 2002. Synthesis and characterization of lanthanum-doped sodium bismuth titanate. Modern Phys. Lett. B16(26): 1007-1019.

Bärnighaus, H. 1979. Group-subgroup relations between space groups: A useful tool in crystal chemistry. Proc. Conf. 'Kristallographische Gruppen', University of Bielefeld, Germany, September 2-16, 1979, p. 139-175.

Beal, K.C. 1987. Precipitation of lead zirconate titanate solid solutions under hydrothermal conditions. In Advances in Ceramics: Ceramic Powder Science I. The Am.Ceram. Soc.Inc. 21: 33-41.

Byrappa, K., and M. Yoshimura. 2001. Handbook of Hydrothermal Technology. A technology for crystal growth and materials processing. Noyes Publications: Park Ridge, NJ, USA.

Carpenter, M.A. 1992. Thermodynamics of phase transitions in minerals: a macroscopic approach. p.172-215 In G.D. Price and N.L. Ross (eds) The Stability of Minerals. Chapman & Hall: London.

Cheng, H., J. Ma, B. Zhu and Y. Cui. 1993. Reaction mechanism in the formation of lead zirconate titanate solid solutions under hydrothermal conditions. J. Am.Ceram.Soc. 76: 625-629.

Cousin, P., and R.A. Ross, 1990. Preparation of mixed oxide: a review. Mater. Sci. & Eng. A130: 119-125.

Cross, L.E. 1993. Ferroelectric Ceramics: Tutorial Reviews, Theory, Processing and Applications. Birkhauser: Basel.

Dawson, W.J. 1988. Hydrothermal synthesis of advanced ceramic powders. Am. Ceram. Soc. Bull. 67: 1673-78.

Dove, M.T., K.O.Trachenko and M.G.Tucker. 2000. Rigid unit modes in framework structures: Theory, experiment and application. p.1-33. In S.A.T. Redfern and M.A. Carpenter (eds) Transformation Processes in Minerals. Reviews in Mineralogy & Geochemistry, Vol. 39, Mineralogical Society of America: Washington D.C.

Eckert, J.O., C.C. Hung-Houston, B.L. Gersten, M.M. Lencka and R.E. Riman. 1996. Kinetics and mechanisms of hydrothermal synthesis of barium titanate. J. Am. Ceram. Soc. 79: 2926-2939.

Groth, P.H.R. von. 1870. Über Beziehungen zwischen Krystallform und chemischer Constitution bei einigen organischen Verbindungen. Ber. Dtsch. Chem. Ges. 3: 449-457.

Heaney, P.J. 2000. Phase transformations induced by solid solution. p.135-174. In S.A.T. Redfern and M.A. Carpenter (eds) Transformation Processes in Minerals. Reviews in Mineralogy & Geochemistry. Vol. 39, Mineralogical Society of America: Washington D.C.

Herabut, A., and A. Safari. 1997. Processing and electromechanical properties of $(Bi_{0.5} Na_{0.5})_{(1-1.5x)}La_xTiO_3$ ceramics. J. Am. Ceram.Soc. 80(11): 2954-2958.

Heywang, W. 1951. Zur wirksamen Feldstärke im kubischen Gitter. Z. Naturforsch. 6a: 219-220.

Heywang, W. 1965. Ferroelektrizität in perowskitischen Systemen und ihre technischen Anwendungen. Z. Angew. Phys. 19: 473-481.

Hosono, Y., K. Harada and Y. Yamashita. 2001. Crystal growth and electrical properties of lead-free piezoelectric material. Jpn. J. Appl. Phys. 40: 5722-5726.

Ichihara, T., T. Tsurumi, K. Asaga, K. H. Lee and M. Daimon. 1999. Hydrothermal synthesis of PZT crystalline powder and piezoelectric properties of ceramics. J. Ceram. Soc. Jpn. Int. Ed. 98: 155-160.

Känzig, W. 1951. Helv. Phys. Acta. 24: 175.

Kay, H.F., and P. Vousdan. 1949. Symmetry changes in barium titanate at low temperature and their relation to its ferroelectric properties. Phil. Mag. 7: 1019-1040.

Kinoshita, K., and A. Yamaji, 1976. Grain size effect on dielectric properties in barium titanate. J. Appl. Phys. 47: 371-373.

Kutty, T.R.N., and R. Balachandran. 1984. Direct precipitation of lead zirconate titanate by the hydrothermal method. Mater. Res. Bull. 19: 1479-1488.

Landau, L.D., and E.M. Lifshitz. 1980. Statistical Physics. 3rd edition, part 1. Pergamon Press: Oxford, New York, Toronto, Sydney, Paris, Frankfurt.

Lee, K.H., K. Asaga, T. Ichihara and M. Daimon. 1987. Synthesis of PZT crystalline powders by reaction of aqueous solution below 200°C. Yogyo Kyokai Shi 95: 74-78 (in Japanese).

Lemoine, L., L. Leriche, P. Tronic and B. Thierry. 1995. Optimization of synthesis parameters of PZT powder through hydrothermal routes. In P. Vincenzine (ed) Advances in Ceramics: Charting the Future. Techn.Ser., The Am.Ceram.Soc.Inc.

Lencka, M.M., A. Andrenko and R.E. Riman. 1995. Hydrothermal precipitation of lead zirconate titanate solid solutions: Thermodynamic modeling and experimental synthesis. J. Am. Ceram. Soc. 78: 2609-2618.

Lencka, M.M., and R.E. Riman. 1995a. Thermodynamics of the hydrothermal synthesis of calcium titanate with reference to other alkaline-earth titanates. Chem. Mater. 7:18-25.

Lencka, M.M., and R.E. Riman. 1995b. Estimation of thermochemical properties for ceramic oxides: A focus on PbZrO3. Thermochim. Acta 256: 193-203.

Lin, C.H., S.C. Pei and T.S. Chin. 1993. Hydrothermal synthesis of $PbTi_{1-x}Zr_xO_3$ ceramic powder. In: Ceramic Transactions, Dielectric Ceramics: Processing, Properties and Applications. 32: 261-274.

Megaw, H.D. 1973. Crystal structures: A Working Approach. Saunders Co.: Philadelphia, p.282-283.

Moulson, A.J., and J.M. Herbert. 1990. Electroceramics. Materials, properties, applications. Chapman & Hall: London, Weinheim, New York, Tokyo, Melbourne, Madras.

Nagata, H., and T. Takenaka. 1997. Lead-free piezoelectric ceramics of $(Bi_{1/2}Na_{1/2})TiO_3 - \frac{1}{2}(Bi_2O_3 Sc_2O_3)$ system. Jpn. J. Appl. Phys. 36: 6055-6057.

Newnham, R.E., and G.R. Ruschau. 1991. Smart electroceramics. J. Am.Ceram.Soc. 74(3): 463-480.

Nord, G.L. Jr. 1994. Transformation-induced twin boundaries in minerals. Phase Trans. 48: 107-134.

Nualpralaksana, S., S. Phanichphant, M. Hengst and R.B. Heimann. 2001. Hydrothermal synthesis of lead zirconate titanate (PZT) and lead lanthanum zirconate titanate (PLZT) nanopowders. cfi/Ber.DKG 78(5):E34-38.

Ponton, C.B. 1993. An overview of hydrothermal and emulsion processing of multiphase ceramic precursor solids. p. 189-194. In P. Duran and J.F. Fernandez (eds) Third Euro-Ceramics, Processing of Ceramics.

Pookmanee, P., S. Phanichphant and R.B. Heimann. 2001. Synthesis and properties of bismuth sodium titanate (BNT). Part I: Chemical synthesis of fine single-phase bismuth sodium titanate powders. cfi/Ber.DKG 78(7): E27-30.

Pookmanee, P., S. Phanichphant, U. Straube and R.B. Heimann. 2003. Synthesis and properties of bismuth sodium titanate (BNT). Part II: Dielectric properties of sintered BNT and La-doped BNT. cfi/Ber. DKG 80(11): E41-44.

Riman, R.E., M.M. Lencka, L.E. McCandlish, B.L. Gersten, A. Andrenko and S.B. Cho. 1996. Intelligent engineering of hydrothermal reactions. In: Proc. 2nd Intern. Conf. Solvothermal Reactions. Dec 18-20, 1996. Takamatsu, Japan. pp. 148-151

Riman, R.E., M.M. Lencka, L.E. McCandlish, B.L. Gersten, A. Andrenko and S.B. Cho. 1997. Intelligent engineering of hydrothermal reactions. p. 74-78. In D.A. Palmer and D.J. Wesolowski (eds) Proc. 5th Intern. Symp. Hydrothermal Reactions. Gatlinburg, Tenn., USA.

Sasaki, A., T. Chiba, Y. Mamiya and E. Otsuki. 1999. Dielectric and piezoelectric properties of $(Bi_{0.5}Na_{0.5})TiO_3-(Bi_{0.5}K_{0.5})TiO_3$ systems. Jpn. J. Appl. Phys. 38: 5564-5567.

Schmidt, V.H., C.-S. Tu and I.G. Siny. 1994. Dielectric and Brillouin anomalies in an $Na_{1/2}Bi_{1/2}TiO_3$ (NBT) relaxor ferroelectric crystal. Proc. IEEE 9th Int. Symp. Appl. Ferroelectr. 45-48.

Skinavi, G.I., I.M. Ksendzov, V.A. Trigubenko and V.G. Prokhvatilov. 1961. Sov. Phys. Solid State (Engl. Transl.) 2(11): 2584.

Smolenskii, G.A., V.A. Isupov, A.I. Agranovskaya and N.N. Krainik. 1961. New ferroelectrics of complex compositions IV. Sov. Phys. Solid State (Engl. Transl.) 2 (11): 2651-2654.

Su, B. 1997. Novel fabrication processing for improved lead zirconate titanate (PZT) ferroelectric ceramic materials. Ph.D. thesis, Faculty of Engineering, The University of Birmingham, UK.

Takenaka, T., and K. Sakata.1989. Dielectric, piezoelectric and pyroelectric properties of $(BiNa)_{1/2}TiO_3$ based ceramics. Ferroelectrics 106: 375-380.

Tautz, F.S., V. Heine, M.T. Dove, and X. Chen. 1991. Rigid unit modes in the molecular dynamics simulation of quartz and the incommensurate phase transition. Phys. Chem. Minerals 18: 326-336.

Thom, R. 1993. Structural stability and morphogenesis: An outline of a General Theory of Models. Reading, MA: Addison-Wesley.

Uchino, K. 1994. Ferroelectric ceramics. p. 635-677. In R.W.Cahn, P.Haasen and E.J.Kramer (eds) Materials Science and Technology. Vol. 11, Structure and Properties of Ceramics.

Wada, T., K. Toyoike, Y. Imanaka and Y. Matsuo. 2001. Dielectric and piezoelectric properties of $(A_{0.5}Bi_{0.5})TiO_3 - ANbO_3$ (A = Na, K) systems. Jpn. J. Appl. Phys. 40: 5703-5705.

Yoshimura, M., and H. Suda. 1994. Hydrothermal processing of hydroxyapatite: Past, present, and future. p. 45-72. In P.W.Brown and B. Constanz (eds) Hydroxyapatite and related materials. CRC Press Inc.